Balance of microtubule stiffness and cortical tension determines the size of blood cells with marginal band across species

Serge Dmitrieff,[1] Adolfo Alsina,[1] Aastha Mathur,[1] and François Nédélec[1]

[1] *Cell Biology and Biophysics Unit, European Molecular Biology Laboratory, Meyerhofstrasse 1, 69117 Heidelberg, Germany.*

(Dated: This manuscript was compiled on November 2, 2016)

The fast blood stream of animals is associated with large shear stresses. Consequently, blood cells have evolved a special morphology and a specific internal architecture allowing them to maintain their integrity over several weeks. For instance, non-mammalian red blood cells, mammalian erythroblasts and platelets have a peripheral ring of microtubules, called the marginal band, that flattens the overall cell morphology by pushing on the cell cortex. In this article, we model how the shape of these cells stems from the balance between marginal band elasticity and cortical tension. We predict that the diameter of the cell scales with the total microtubule polymer, and verify the predicted law across a wide range of species. Our analysis also shows that the combination of the marginal band rigidity and cortical tension increases the ability of the cell to withstand forces without deformation. Finally, we model the marginal band coiling that occurs during the disc-to-sphere transition observed for instance at the onset of blood platelet activation. We show that when cortical tension increases faster than crosslinkers can unbind, the marginal band will coil, whereas if the tension increases slower, the marginal band may shorten as microtubules slide relative to each other.

arXiv:1610.10035v2 [q-bio.SC] 1 Nov 2016

The shape of animal cells is determined by the cytoskeleton, including microtubules (MTs), contractile networks of actin filaments, intermediate filaments and other mechanical elements. The 3D geometry of most cells in a multi-cellular organism is also largely determined by their adhesion to neighbouring cells or to the extra-cellular matrix [1]. This is not however the case for blood cells as they circulate freely within the fluid environment of the blood plasma. Red blood cells (RBC) and thrombocytes in non-mammalian animals [2, 3], platelets and erythroblasts in mammals [4, 5] adopt a simple ellipsoidal shape (Fig. 1A). This shape is determined by two components: a ring of MTs, called the marginal band (MB), and a protein cortex at the cell periphery.

In the case of platelets and non-mammalian red blood cells, both components are relatively well characterized (Fig. 1). The cortex is a composite structure made of spectrin, actin and intermediate filaments (Fig. 1B), and its complex architecture is likely to be dynamic [11–13]. It is a thin network under tension [14], that on its own would lead to a spherical morphology [15]. This effect is counterbalanced by the MB, a ring made of multiple dynamic MTs, held together by crosslinkers and molecular motors into a closed circular bundle [4, 16] (Fig. 1C). The MB is essential to maintain the flat morphology, and treatment with a MT destabilising agent causes platelets to round up [17]. It was also reported that when the cell is activated, the MB is often seen to buckle [3]. This phenomenon is reminiscent of the buckling of a closed elastic ring [18], but the MB is not a continuous structure of constant length.

Indeed, an important feature of the MB is that is it made of multiple MTs, connected by dynamic crosslinkers. The rearrangement of connectors could allow MTs to slide relative to one another, and thus would allow the length of the MB to change. Secondly, MT growth or depolymerisation would also induce reorganisation. However, in the absence of sliding, elongation or shortening of single MTs would principally affect the thickness of the MB (*i.e.* the number of MT in the cross-section) rather than its length. It was also suggested that molecular motors may drive the elongation of the MB [19], but this possibility remains mechanistically unclear. These aspects have received little attention so far, and much remains to be done before we can understand how the original architecture of these cells is adapted to their unusual environment, and to the mechanical constraints associated with it [7].

We argue here that despite the potential complexity of the system, the equilibrium between MB elasticity and cortical tension can be understood in simple mechanical terms. We first predict that the main cell radius should scale with the total length of MT polymer and inversely with the cortical tension, and test the predicted relationship using data from a wide range of species. We then simulate the shape changes observed during platelets activation [20], discussing that a rapid increase of tension leads to MB coiling accompanied by a shortening of the ring, while a slow increase of tension leads to a shortening of the ring without coiling. Finally, by computing the buckling force of a ring confined within an ellipsoid, we find that the resistance of the cell to external forces is dramatically increased compared to the resistance of the ring alone.

RESULTS

Cell size is controlled by total microtubule polymer and cortical tension

We first apply scaling arguments to explore how cell shape is determined by the mechanical equilibrium between MB elasticity and cortical tension. In their rest-

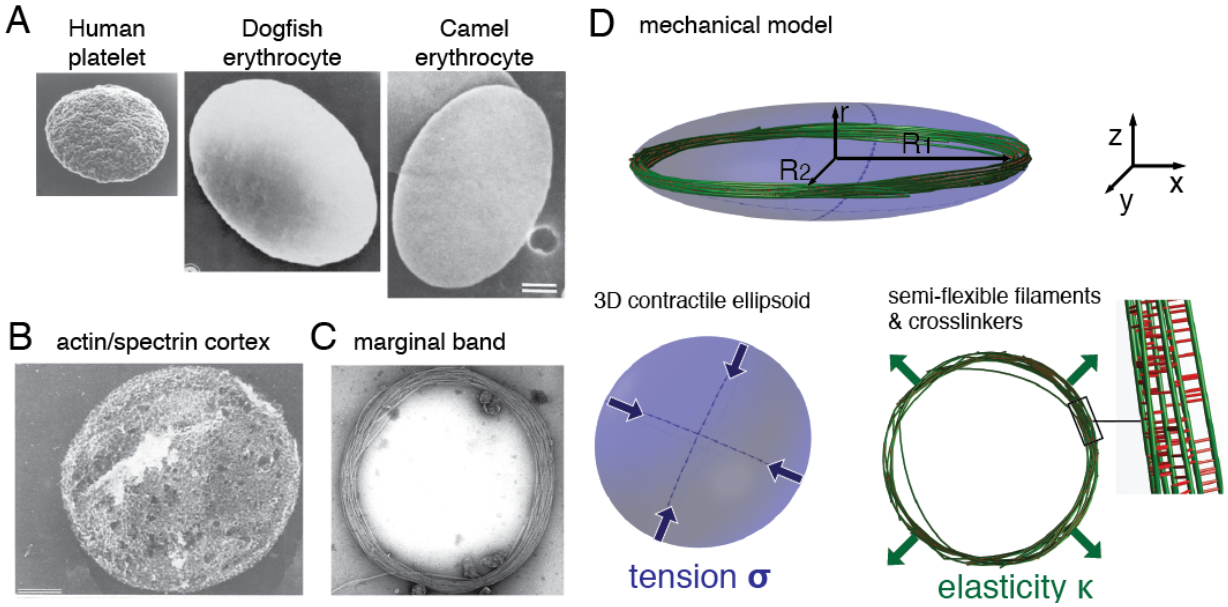

FIG. 1. A) Scanning electron micrographs of Platelets and Erythrocytes shown at the same scale [6–8], scale bar $1\mu m$. B) The actin/spectrin cortex of platelets, EM from [9], scale bar $0.5\mu m$. C) The MB of platelets is made of multiple MTs bundled by motors and crosslinkers [10], EM from [6]. D) In our model, the shape of the cell is determined by the balance of two forces. Because of microtubule stiffness κ, the MB pushes against the tense cortex, which resists by virtue of its surface tension σ.

ing state, the cells are flat ellipsoids and the MB is contained in a plane that is orthogonal to the minor cell axis. Assuming that the cell is discoid for simplicity ($R_1 = R_2 = R$) the major radius R is also approximately the radius of the MB (Fig 1D), and thus the MTs bundled together in the MB have a curvature $\sim 1/R$. We first consider timescales larger than the dynamics of MT crosslinker binding and unbinding (about 10 seconds [21]), for which we can ignore the mechanical contribution of crosslinkers [10]. Using the measured flexural rigidity $\kappa = 22\,pN\mu m^2$ of MTs [22], and defining $\mathcal{L}$ as the sum of all MTs length, the elastic energy of the MB is $E_B = \frac{\kappa}{2}\mathcal{L}/R^2$. At time scales larger than a few seconds, the cortex can reorganize and therefore we do not have to consider its rigidity [23]. Its effect can then be modeled by a surface energy associated with a surface tension σ (Fig 1D). The surface area is $S = 2\pi R^2[1 + O(\frac{r}{R})]$, in which $2r$ is the thickness of the cell. Assuming the cell to be flat enough, its surface area is therefore approximately $2\pi R^2$ and the energy is $E_T \sim 2\pi\sigma R^2$. The equilibrium of the system corresponds to $\partial_R(E_B + E_T) = 0$, leading to :

$$R^4 = \frac{\kappa\mathcal{L}}{4\pi\sigma}\,. \tag{1}$$

All other things constant, we thus expect $R \propto \mathcal{L}^{1/4}$. To verify this relationship, we compiled data from 25 species available from the literature [2], computing $\mathcal{L}$ by multiplying the number of microtubules in a cross-section by the length of the marginal band. The scaling is remarkably respected, over more than two orders of magnitudes (Fig. 2A). Using equation 1, the fit provides an estimate of the tension of $\sigma \sim 0.1pN/\mu m$, which is low compared to the tension $\sigma \sim 100pN/\mu m$ of the actomyosin cortex of blebbing cell [24]. However, RBC have a cortex made of spectrin rather than actomyosin, and thus have a much lower tension, that compensates a negative membrane tension [25]. In Human RBC, membrane tension was shown to be negative with a magnitude of $0.65\,pN/\mu m$ [26], close to the magnitude derived from our theory. In contrast to RBC, we predict $\sigma = 40\,pN/\mu m$ for Human blood platelets, given that $R \approx 2\mu m$ and $\mathcal{L} \approx 100\mu m$ [27], which is close to the value reported for blood granulocytes ($35\,pN/\mu m$) [14].

The precise scaling observed in the experimental data confirms our mechanically driven hypothesis where the MB pushes on the cell cortex, and in which at long time scales (on the order of a minute), only the bending rigidity of the MTs and the cortical tension need to be considered (Fig 1D). To verify that this result is still valid for a ring of multiple dynamically crosslinked MTs, we developed a numerical model of cells with MBs in *Cytosim*, a cytoskeleton simulation engine [28]. *Cytosim* simulates stochastic binding/unbinding of connectors, and represents them by a Hookean spring between two MTs. For this work, we extended *Cytosim* to be able to model a contractile surface under tension that can be deformed by the MTs. Cell shape is restricted to remain ellipsoidal, and is described by six parameters: three axes length R_1, R_2, r and a rotation matrix, *i.e.* three angles. The three lengths are constrained such that the volume of the ellipsoid remains constant. To implement confinement, any MT model-point located outside the cell is subject to inward-directed force $\mathbf{f} = k\delta$, in which δ is the

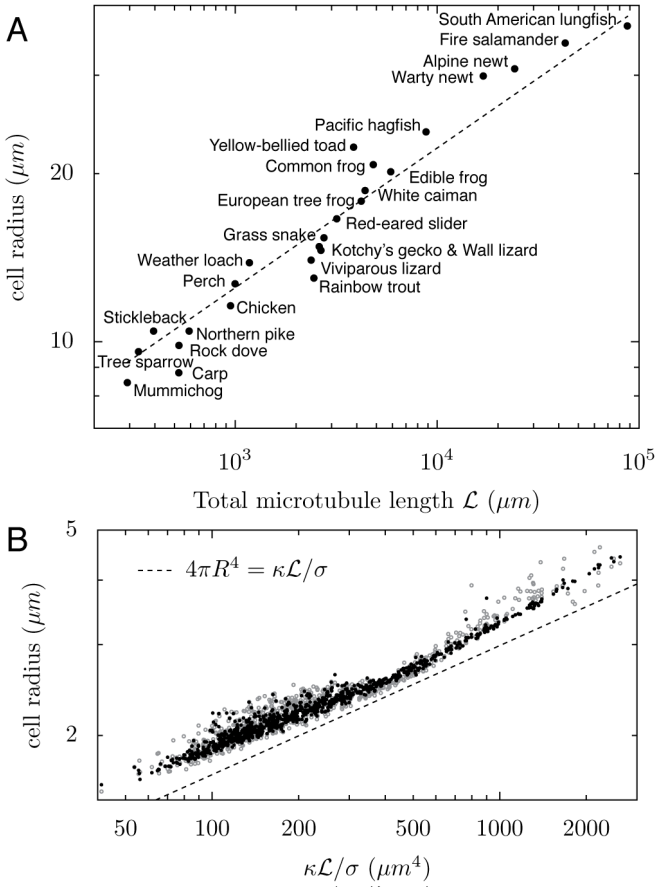

FIG. 2. A) Cell radius as a function of total MT length $\mathcal{L}$. Dots: data from 25 species ([2]). $\mathcal{L}$ was estimated from the number of microtubules in a cross-section, measured in electron microscopy, and the cell radius. B) Cell radius as a function of $\mathcal{L}\kappa/\sigma$ in simulations with 0 (gray points) or 10000 (black points) crosslinkers. On both graphs, the dashed line indicates the theory $4\pi R^4 = \kappa\mathcal{L}/\sigma$.

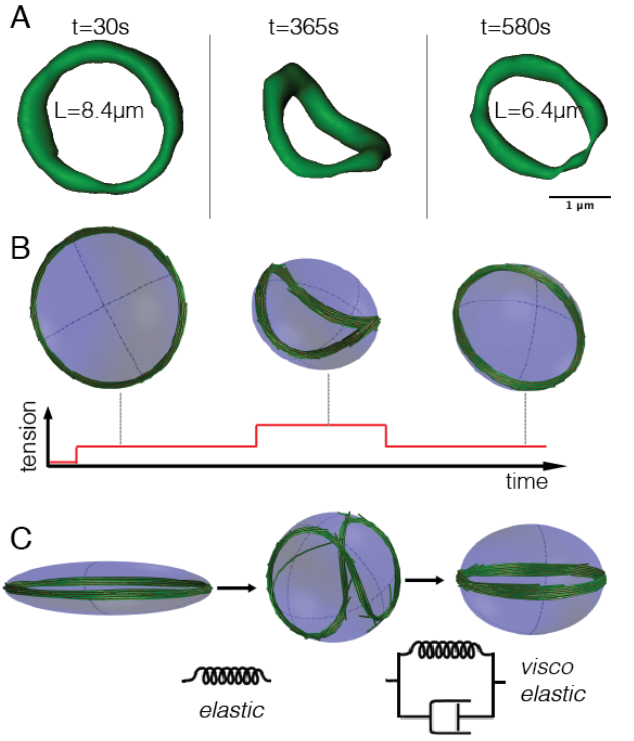

FIG. 3. A) MB of a live platelet labeled with SIR-tubulin dye. Fluorescence images were segmented at the specified time after the addition of ADP, a platelet activator, to obtain the MB size L. B) Simulation of a platelet at different times. A limited increase of the tension ($90pN/\mu m$) causes the MB to shorten while a large increase of the tension ($220pN/\mu m$) causes the buckling of the MB. C) Simulations show that if cell rounding is fast enough, the MB buckles because crosslinkers cannot reorganize. This represent an elastic behavior, but at longer times, the MB rearranges, leading to a viscoelastic response.

shortest vector between the point and the surface and k the confining stiffness. Here for each force $\mathbf{f}$ applied on a MT, an opposite force $-\mathbf{f}$ is applied to the surface, in agreement to Newton's third law. The rates of change of the ellipsoid parameters are then given by the net force on each axis, divided by μ, an effective viscosity parameter (see Suppl. 1.I.A). The value of μ affects the rate of cell shape change but not the stationary cell shape. This approach is much simpler than using a tessellated surface to represent the cell, and still general enough to capture the shape of blood platelets [3, 29] and several RBCs [8, 30], see Fig. 1A.

To model resting platelets, we simulated a ring made of 10–20 MTs of length 9–16μm [4] with 0 or 10000 crosslinkers, confined in a cell of volume $8.4\mu m^3$ with a tension $\sigma \sim 0.45$–$45pN/\mu m$, for over six minutes, until equilibration. We find that the numerical results agree with the scaling law, over a very large range of parameter values as illustrated in Fig. 2B. Interestingly, we find that simulated cells are slightly larger than predicted analytically. This is because MTs of finite length do not exactly follow the cell radius, and their ends are less curved, thus exerting more force on the cell. This means that the value of the tension we computed from the biological data ($\sigma \sim 0.1pN/\mu m$) is slightly under-estimated. More importantly, the simulation shows that with or without crosslinkers, the cell has the same size at equilibrium (compare black and gray dots on Fig. 2B), confirming that, because they can freely reorganize, crosslinkers should not affect the long-term elasticity of the MB. To understand the mechanics of blood cells with MBs at short time scale, however, it is necessary to consider the crosslinkers.

The marginal band behaves like a viscoelastic system

During activation, mammalian platelets round up before spreading, and their MB coils during this process which occurs within a few seconds [19]. Similar reports were made for thrombocytes [3]. To observe these re-

sults experimentally, we extracted mice platelets, and activated them by exposing them to adenosine diphosphate ADP, causing an often reversible response. By monitoring the MB with SiR-tubulin, a bright docytaxe-based MT dye, we could capture the MB coiling live, Fig. 3A. As it coils, the MB adopts the shape of the baseball seam curve, which is the shape that an incompressible elastic ring would adopt when constrained into a sphere smaller than its natural radius [31]. Thus, at short time scale, the MB seems to behave as an incompressible ring, and we reasoned that this must be because crosslinkers prevent MTs from sliding relative to each other. To analyse this process further, we returned to *Cytosim*. After an initialisation time, in which the MB assembles as a ring of MTs connected by crosslinkers, cortical tension is increased stepwise. The cell as a consequence becomes spherical, and, because its volume is conserved, the largest radius is reduced compared to that of the discoid resting state. As a result, the MB adopts a baseball seam shape (Fig. 3B). Over a longer period, however, the MB regained a flat shape, as MTs rearranged into a new, smaller, ring (Fig. 3A). In conclusion, the simulated MB is viscoelastic (Fig. 3B). At short time scales, MTs do not have time to slide, and the MB behaves as an incompressible elastic ring. At long time scales, the MB behaves as if crosslinkers were not present, with an overall elastic energy that is the sum of individual MT energies. Thus overall, the ring seems to transition from a purely elastic at short time scales, to a viscoelastic Kelvin-Voigt law at long time scales (Fig. 3C). The transition between the two regimes is determined by the timescale at which crosslinkers permit MTs to slide.

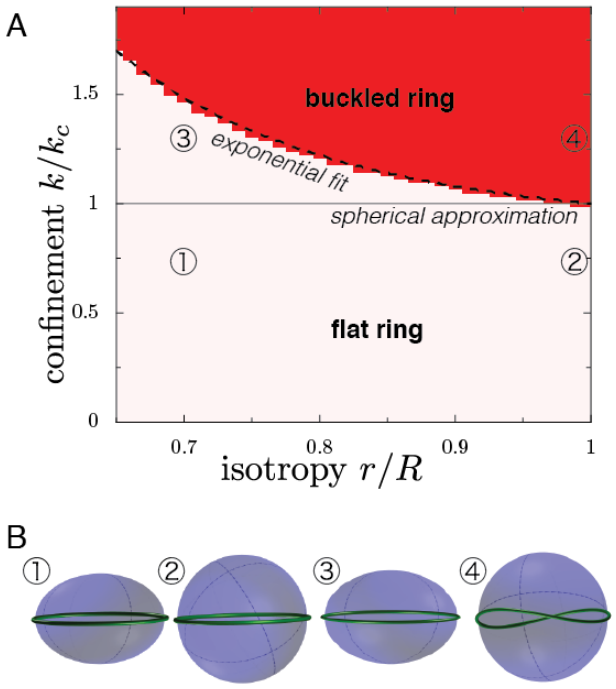

FIG. 4. A) Degree of coiling as a function of normalized confinement stiffness k/k_c and isotropy r/R of the fixed oblate ellipsoid in which the ring is confined. The light shade indicates regions of uncoiled states and the red area indicates coiled states, as determined by simulations. The dashed line represents the empirical function $k^* = k_c(\frac{r}{R})^2 e^{\alpha(1-\frac{R}{r})}$, where $\alpha = 2.587$ is a phenomenological parameter that depends on ϵ, itself defined from the MB length as $L = 2\pi R(1+\epsilon)$. B) Illustrations of MB shapes in different regimes, as indicated by the circled numbers.

The cell is unexpectedly robust

The MB in blood cells is necessary to establish a flat morphology, but also to maintain this morphology in face of transient mechanical challenges, for example as the cell passes through a narrow capillary [7]. In this section, we calculate the response of a cell to a fast mechanical stimuli during which crosslinkers do not reorganize. Therefore, we can assume that the ring is uniform and of constant length, to investigate how cortical tension affects the resistance of the cell to coiling. Firstly, we examine the mechanics of a closed ring of length L and rigidity κ_r within a sphere, and then extend these results to a non-deformable ellipsoid. The shape of a ring in a sphere was previously calculated numerically [31], and we extended these result by deriving analytically the force f_B required to buckle a confined ring (see Suppl. 1.II.B). If E_B is the energy of a buckled MB, the force is :

$$f_B = -\lim_{L\to 2\pi R} \partial_R E_B = 8\pi \frac{\kappa_r}{R^2} \qquad (2)$$

We verified this relation in simulations, with $L = 2\pi R(1+\epsilon)$, where $1 \gg \epsilon > 0$, which made the ring slightly oversized compared to its confinement. Given the confining stiffness k, the force applied to each model-point of the ring is $kR\epsilon$. If n is the number of model-points in the rings (*i.e.* $n = L/s$ where s is the segmentation), the total centripetal force is $nkR\epsilon$. Hence, we expect that the ring will buckle if k exceeds $k_c = \frac{1}{nR\epsilon} f_B$. Upon systematically varying k in the simulation (see Methods), we indeed found that the ring coils for $k > k_c$, Fig. 4A. We next simulated oblate ellipsoidal cells, with $R_1 = R_2 = R$ and $r < R$, and we varied the flatness of the cell by changing r/R. We found that the measured critical confinement k^* is indeed k_c for $r = R$, but increases exponentially with $1 - R/r$, Fig. 4. The buckling force of a MB is thus much higher when the MB is confined. This is important mechanically, as it implies that the flat state of the MB should be metastable, and this could make a blood platelet 50 times more resilient to buckling (assuming an isotropy ratio $r/R = 0.25$).

Coiling stems from cortical tension overcoming MB rigidity

We can now consider the case of a ring inside a deformable ellipsoid of constant volume $V_0 = 4/3\pi R_0^3$, gov-

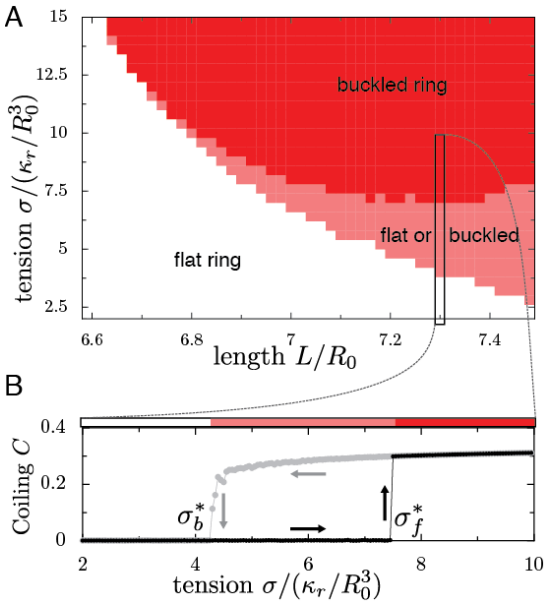

FIG. 5. A) Configuration of the MB as a function of renormalized tension $\sigma R_0^3/\kappa_r$ and renormalized MB length L/R_0, in which the volume of the cell is $\frac{4}{3}\pi R_0^3$. The state of the MB is indicated by colours: gray: flat MB ; red : always buckled MB ; pink : bistable region, in which the MB can be either buckled or flat. B) A cut through the phase diagram, for a MB of length $L = 7.3R_0$. The degree of coiling (see methods for definition) as a function of tension, in a cell initially flat (black dots) or buckled (gray dots), shows the metastability of the flat state. Arrows illustrate the hysteresis.

erned by a surface tension σ. The length of the ring L is set with $L > 2\pi R_0$, such that we expect the ring to remain flat, at low tension, and to be coiled, at high tension, because it does not fit in the sphere of radius R_0. In simulations, starting from a flat ring, we observe as predicted the existence of a critical tension σ_f^* leading to buckling, Fig. 5A. This shows that increasing $\sigma R_0^3/\kappa_r$, *i.e.* increasing the ratio of cortical tension over ring rigidity, leads to cell rounding. Thus, either increasing the cortical tension or weakening the ring will lead to coiling. Starting from a buckled ring, decreasing the tension below a critical tension σ_b^* also leads to the cell flattening, as predicted. However, our simulations show that $\sigma_b^* < \sigma_f^*$: a cell initially flat will remain flat for $\sigma_b^* < \sigma < \sigma_f^*$, while a cell initially round will remain round for $\sigma_b^* < \sigma < \sigma_f^*$, Fig. 5A,B. Hysteresis is the hallmark of bistability, and we had predicted this bistability in the previous section by showing that the flat configuration is metastable. This metastability, *i.e.* the fact that a MB in a flat cell has a higher buckling threshold than in a spherical cell, allows the cell to withstand very large mechanical constraints such as shear stresses.

DISCUSSION

We have examined how the forces determining the morphology of blood cells balance each other. In particular, we predicted a scaling law $4\pi R^4 = \kappa\mathcal{L}/\sigma$, if the elasticity of MTs is compensated by cortical tension, in which $\mathcal{L}$ is the sum of the lengths of the MTs inside the cell, κ the bending rigidity of MTs and σ the cortical tension. Remarkably, this scaling law is well respected by values of R and $\mathcal{L}$ measured for 25 species. We caution that these observations were made for non-discoidal RBC (where the two major axes differ), indicating that other factors not considered here must be at work [7]. In human RBC, perturbation of the spectrin meshwork can lead to elliptical RBC [32], showing that the cortex can impose anisotropic tensions, while another study suggests that MB-associated actin can sequester the MB into an elliptical shape [33]. Cortical anisotropy would be an exciting topic for future studies, but this may not be needed to understand wild-type mammalian platelets.

Using analytical theory and numerical simulations, we analyzed the mechanical response of cells with MB, and showed a complex viscoelastic behavior characterized by a timescale τ_c that is determined by crosslinker reorganization. At long time scales ($t \gg \tau_c$), the MB behaves elastically, and its elasticity is the sum of all MTs rigidity. At short time scales ($t < \tau_c$), the MB behaves as an incompressible elastic ring of fixed length because crosslinkers do not yield. At this time scale, the stiffness of the ring exceeds the sum of the individual MT stiffness as long as the crosslinkers connect neighboring MT tightly [34]. Buckling leads to the baseball seam curve, which is a configuration of minimum elastic energy. This explains the coiled shape of the MB observed in mouse platelets, as well human platelets [19] and well as dogfish thrombocytes [3]. Thus an increase of cortical tension over bundle rigidity can cause coiling, if the cell deforms faster than the MB can reorganize. A fast increase of tension is a likely mechanism supported by several experimental evidence [35–37]. In dogfish thrombocytes and platelets, blebs are concomitant with MB coiling, suggesting a strong increase of cortical tension [3]. We note however that a recent study suggests that MB destabilization could be due to ring extension [19].

Finally, calculating the buckling force of a cell containing an elastic MB and a contractile cortex led to a surprising result. We found that the buckling force increased exponentially with the cell flatness, because the cortex reinforces the ring laterally. This makes the marginal band a particularly efficient system to maintain the structural integrity of blood cells. For transient mechanical constraints, the MB behaves elastically and the flat shape is metastable, allowing the cell to overcome large forces without deformation. However, as we observed, the viscoelasticity of the MB allows the cell to adapt its shape when constraints are applied over long timescales, exceeding the time necessary for MB remodeling by crosslinker binding and unbinding. This study

suggest that it will be particularly interesting to compare the time-scale at which blood cells experience mechanical stimulations *in vivo*, with the time scale determined by the dynamics of the MT crosslinkers.

METHODS

MTs of persistence length l_p are described as bendable filaments of rigidity $\kappa = k_B T l_p$, in which $k_B T$ is the thermal energy. We can write the energy of such a filament of length L as the integral of its curvature squared :

$$E = \frac{\kappa}{2} \int_0^L \left(\frac{d^2 \mathbf{r}}{ds^2} \right)^2 ds \tag{3}$$

Where $\mathbf{r}(s)$ is the position as a function of the arclength s along the filament. The dynamics of such a system was simulated in Cytosim, an Open Source simulation software [28]. In Cytosim, a filament is represented by model points distributed regularly defining segments of length s. Fibers are confined inside a convex region of space Ω by adding a force to every model points that is outside Ω. The force is $\mathbf{f} = k(\mathbf{p} - \mathbf{r})$, where $\mathbf{p}$ is the projection of the model point $\mathbf{r}$ on the edge of Ω. For this work, we implemented a deformable elliptical surface confining the MTs, parametrized by six parameters. The evolution of these parameters is implemented using an effective viscosity (see Suppl. 1.I.C). To verify the accuracy of our approach, we first simulated a straight elastic filament, which would buckle when submitted to a force exceeding $\pi^2 \kappa / L^2$, as shown by Euler. Cytosim recovered this result numerically. For a closed circular ring, we also find that the critical tension necessary for buckling corresponds very precisely to the theoretical prediction [38]. This is also true for an elastic ring confined inside a prolate ellipsoid of tension σ (see Suppl. 1.I.D).

To simulate cell radius as a function of $\mathcal{L}\kappa/\sigma$, we used a volume of $8\pi/3 \mu m^3$ (close to the volume of a platelet), with a tension $\sigma \sim 0.45$–$45 pN/\mu m$, consistent with physiological values. The MTs have a rigidity $22\, pN\, \mu m^2$ as measured experimentally [22]. We simulate $10 - 20$ MTs of length $9 - 16 \mu m$, and with a segmentation of $125 nm$, we used more than 70 points per MTs. The crosslinkers have a resting length of $40 nm$, a stiffness of $91 pN/\mu m$, a binding rate of $10 s^{-1}$, a binding range of $50 nm$, and an unbinding rate of $6 s^{-1}$. An example of simulation configuration file is provided in Suppl. 2. When considering an incompressible elastic ring, we used a cell of volume $4/3\pi R_0^3$, where R_0 is the radius of the resting (spherical) cell. For simplicity, we can renormalize all lengths by R_0 and thus all energies by κ_R / R_0. We simulate a cell with a tension $\sigma = 5 - 18 \kappa_R / R_0^3$, and a ring of length $1 - 1.2 \times 2\pi R_0$. To test the effect of confinement, we place an elastic ring of rigidity κ in an ellipsoid space of radii R_0, R_0, $r\, R_0$, in which $r < 1$. The elastic ring has a length $(1 + \epsilon) 2\pi R_0$, in which $\epsilon = 0.05$. To describe how coiled is a MB, we first perform a principal component analysis using all the MTs model points. The vector $\mathbf{u}_z$ is then set in the direction of the smallest eigenvalue while $\mathbf{u}_x, \mathbf{u}_y$ are set orthogonally. We can then define the degree of coiling C as the deviation in Z divided by the deviations in XY:

$$C = \sqrt{\frac{\sum z^2}{\sum x^2 + y^2}} \tag{4}$$

Thus, C is independent of the size of the cell and only measures the deformation of the MB. To measure the critical value of a parameter μ (e.g. tension or confinement) leading to coiling, we computed the derivative of the degree of coiling C with respect to this parameter. Because buckling is analogous to a first-order transition, the critical value μ^* can be defined by :

$$\partial_\mu C \big|_{\mu^*} = \max \|\partial_\mu C\| \tag{5}$$

Platelets were extracted using a previously published protocol [39], and labeled by SiR-tubulin [40] purchased from Spirochrome.

I. SI I : SIMULATION OF MICROTUBULES/CORTEX INTERACTION

To understand cell shape maintenance, one needs to model the interaction between the cellular cortex and the microtubule marginal band. The structure of the marginal band is well known, compared to the organization of the cortex which is not caracterized. We thus decided to represent the microtubules individually, and the cortex effectively as a contractile surface. The interactions between a discretized (*e.g.* triangulated) surface and discrete filaments can be a demanding problem computationally, since such a surface would have a very large number of degrees of freedom. In contrast, we describe here how the problem remains relatively simple for a continuous shape that is described by a limited number of parameters.

A. General formulation

1. Forces and parametrization

Let $S(p_k)$ be the surface defined by the set of parameters $\{p_k\}_{k<n}$. Let $\{\mathbf{f}_i\}_{i<m}$ be the set of forces applied on S at the points $\{\mathbf{r}_i\}_{i<m}$. They are defined by $-\mathbf{f}_i = \partial E / \partial \mathbf{r}_i$, where E is the energy of the system (excluding the surface). One can define "effective forces" $\{\phi^k\}_{k<n}$ associated with each degree of freedom of the surface :

$$\phi^k = -\frac{\partial E}{\partial p_k} = \sum_{i<m} \mathbf{f}_i . \frac{\partial \mathbf{r}_i}{\partial p_k} \tag{6}$$

We can define δE the infinitesimal change in energy after an infinitesimal set of displacements $\delta \mathbf{r}_i$, and then compute it as a function of the infinitesimal set of parameter

changes δp_k.

$$\delta E = -\sum_i \delta \mathbf{r}_i . \mathbf{f}_i \tag{7}$$

$$\delta \mathbf{r_i} = \sum_k \delta p_k \frac{\partial \mathbf{r}_i}{\partial p_k} \tag{8}$$

$$\delta E = -\sum_k \delta p_k \phi^k \tag{9}$$

To write equation 8, we had to assume that any displacement of the surface (allowed by the constraints) can be described in terms of p_k, i.e. that $S(\{p_k\})$ is surjective. It is here interesting to notes that ϕ^k has the dimension of a force if p_k is a length, while it has the dimention of a torque (i.e. an energy) is p_k is an angle.

2. Constraints

In many cases, constraints can be introduced using Lagrange multipliers, by inserting them into the energy E. For instance, to maintain the volume, we can define an energy $E' = E + PV$ where V is the volume and P is the pression ; here P is also a Lagrange multiplier and we have to calculate its value appropriately to obtain $V = V_0$. The pseudo-forces ϕ^k_P associated to pressure are :

$$\phi^k_P = -P \frac{\partial V}{\partial p_k} \tag{10}$$

B. Contractile Ellipsoid

In this section, we describe a more complex, 3D surface. We model an ellipsoid centered around 0 that has a fixed volume V_0 and a a surface tension σ, which means an energy $E_n = \sigma S$, where S is the surface area of the ellipsoid. The ellipsoid is described by its eigenvectors $\mathbf{u}_{1,2,3}$ and their eigenvalues (i.e. the radii of the ellipse) $a_{1,2,3}$. We will also use the orientation matrix $M = [\mathbf{u}_1, \mathbf{u}_2, \mathbf{u}_3]$. By construction, M is a rotation matrix of determinant 1.

1. Surface Tension

We can compute the pseudo-forces associated to surface tension as:

$$\phi^k_\sigma = -\sigma \frac{\partial S}{\partial a_k} \tag{11}$$

The surface area of an ellipsoid is a complex special function that is not a combination of the usual functions. For convenience, we used an analytical approximation of the area :

$$S(a_1, a_2, a_3) \simeq 4\pi \left(\frac{(a_1 a_2)^p + (a_3 a_2)^p + (a_1 a_3)^p}{3} \right)^{\frac{1}{p}} \tag{12}$$

For which $p = 1.6075$ is an empirical parameter. This formula yields an error usually below a percent.

2. Point Forces

To add the contribution of the external forces exerted by the microtubules on the surface, we need to determine $\partial \mathbf{r}/\partial p_k$. The position of a point on the surface of the ellipsoid is defined by two angles θ, ϕ as :

$$\mathbf{r} = \mathbf{u}_1 r_1 \cos\theta \sin\phi + \mathbf{u}_2 r_2 \sin\theta \sin\phi + \mathbf{u}_3 r_3 \cos\phi \tag{13}$$

Therefore, we have :

$$\frac{\partial \mathbf{r}}{\partial r_k} = \mathbf{r}.\mathbf{u}_k \tag{14}$$

It is clear that only the component of the force normal to the surface is providing work upon changing r_k, therefore, we can discard the tangential component when computing the radial forces. The contribution of a force $\mathbf{f}$ at a point r with a local normal $\mathbf{n}$ to the pseudo force ϕ^k_f is therefore :

$$\phi^k_f = f_n \frac{\mathbf{n}.\mathbf{u}_k}{\|\mathbf{u}_k\|} \tag{15}$$

$$\text{With : } f_n = \mathbf{f}.\mathbf{n} \tag{16}$$

We can now compute the torque generated by $\mathbf{f}$. In 2D, it would be convenient to describe the ellipse orientation by an angle θ, and the result is that the "angular force" ϕ^θ is the torque $\mathbf{r} \times \mathbf{f}$. We will assume that this is general and stays true in 3D ; thus we can write ϕ^{ang} directly as a vector :

$$\boldsymbol{\phi}^{ang} = \mathbf{r} \times \mathbf{f} \tag{17}$$

a. Volume conservation To implement volume conservation we only need to find a pressure P such that $(V - V_0)/V_0 < \epsilon$ where ϵ is the tolerance. Many techniques allow the convergence to a suitable value of P - and the choice of method has no physical implication. Here we used a gradient descent method known as the shooting method. For this, we start with an initial value of $P = 0$ and we compute $V(P)$. If $V(P) - V_0/V_0 > \epsilon$, we compute $V(P + \delta P)$ to get the gradient of the volume with respect to pressure. We then follow this gradient until we reach the desired aim for V. This method works very well if $V(P)$ is monotonous, which is always the case here.

The volume of the ellipse is $V = \frac{4}{3}\pi a_1 a_2 a_3$ and therefore, using the Lagrange multiplier P to conserve the volume we can write :

$$\phi^k_P = \frac{4}{3}\pi P \frac{a_1 a_2 a_3}{a_k} \tag{18}$$

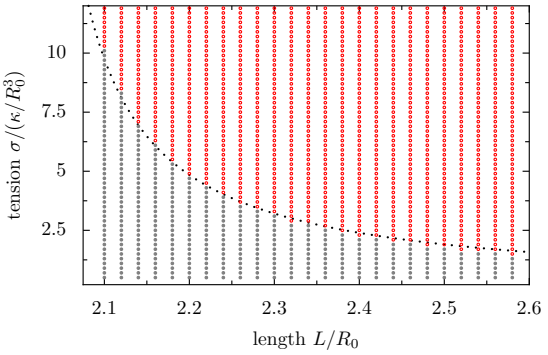

FIG. 6. Phase diagram of the degree of buckling as a function of the length and the tension. Red means that the filament is buckled, gray that it is flat. The dashed line represents the critical tension calculated in Eq. 22.

C. Time Evolution

We can now define the time evolution of the ellipse. We assume a unique viscosity μ associated to the change of size of the ellipse, and a rotational viscosity η_{ang}.

$$\dot{a_k} = \frac{1}{\mu}\left(\phi_P^k + \phi_\sigma^k + \sum \phi_f^k\right) \tag{19}$$

$$\dot{M} = R\left(\mathbf{u}\right) \quad \text{with} \quad \mathbf{u} = \frac{1}{\eta_{ang}} \sum \boldsymbol{\phi}_f^{ang} \tag{20}$$

In which $R(\mathbf{u})$ is the rotation matrix generated from the moment vector $\mathbf{u}$.

D. Simulations Validation

To validate out numerical method and its implementation, we first simulated a microtubule bundle confined inside an ellipsoid cell of tension σ and volume $\frac{4}{3}\pi R_0^3$. A classical result of analytical mechanics is that a filament should buckle under a force tangential force f is this force is larger than a critical force :

$$f_1^* = \frac{\kappa\pi^2}{L^2} \tag{21}$$

Assuming the microtubules to be sliding freely, the critical buckling force of a microtubules is thus $f_n^* = nf_1$. We confined the microtubule in a contractile ellipsoid, which thus takes the shape of a prolate ellipsoid. Let us call $a_1 = R$ the longer axis of this ellipsoid, and the shorter axis are $a_2, a_3 = \sqrt{R_0^3/R}$. The force exerted on the microtubule is $f_\sigma = 2\sigma\partial_R S(R, \sqrt{R_0^3/R}, \sqrt{R_0^3/R})$, with S defined in equation 12. Starting with a microtubule of length L, buckling will occur for a critical tension :

$$\sigma^* = \frac{\kappa\pi^2}{2R^2}\left(\partial_R S(R, \sqrt{R_0^3/R}, \sqrt{R_0^3/R})\right)^{-1} \tag{22}$$

II. SI II : MECHANICS OF A CONFINED RING

A. Formulation

Let us consider a rod of length L lying on a sphere of radius R. We can describe this rod by its position $\mathbf{r}$, parametrized by its arclength s, such that the energy reads :

$$E(R, L) = \frac{\kappa}{2}\int_0^L \ddot{\mathbf{r}}^2 ds \tag{23}$$

Because the rod lies on the unit sphere, and because s is the arclength, we have the constraints :

$$\|\mathbf{r}\|^2 = R^2 \qquad \text{and} \qquad \|\dot{\mathbf{r}}\|^2 = 1 \tag{24}$$

We can introduce this as constraints in the energy using two Lagrange multipliers α and β, to define :

$$E = \frac{\kappa}{2}\int_0^L \left[\ddot{\mathbf{r}}^2 + \alpha(R^2 - \|\mathbf{r}\|^2) + \beta(\|\dot{\mathbf{r}}\|^2 - 1)\right] ds \tag{25}$$

Minimizing this energy yields the Euler-Lagrange equation :

$$\mathbf{r}^{(4)} = \alpha\mathbf{r} + \dot{\beta}\dot{\mathbf{r}} + \beta\ddot{\mathbf{r}} \tag{26}$$

Since the curve is lying on a sphere, we can use the identity :

$$\ddot{\mathbf{r}}(s) = k_i(s)\left[\mathbf{r}(s) \times \dot{\mathbf{r}}(s)\right] - \frac{1}{R^2}\mathbf{r}(s) \tag{27}$$

In which $k(i)$ is the intrinsic (geodesic) curvature. Eventually, we find :

$$\ddot{k_i} = \frac{k_i}{R^2}\left(\gamma - \frac{R^4}{2}k_i^2\right) \tag{28}$$

In which γ is a constant [31]. To find the shape of a closed ring, one needs to find the value of α and $k_i(0)$ such that the curve is of length L is a closed ring, i.e. :

$$\mathbf{r}(L) = \mathbf{r}(0) \quad \text{and} \quad \dot{\mathbf{r}}(L) = \dot{\mathbf{r}}(0) \tag{29}$$

Numerically, we determined γ and $k_i(0)$ using a shooting method.

B. Weakly deformed ring

For a weakly deformed ring, equation 28 can be simplified to

$$\ddot{k_i} = \frac{\gamma}{R^2}k_i \tag{30}$$

Periodicity imposes $\sqrt{-\gamma} \to m$ when $L \to 2\pi R$, in which $m \in \mathbb{N}$. Since the lowest energy curve has a period $L/2$, we can conclude that $m = 2$, i.e. $\gamma \to -4$ for

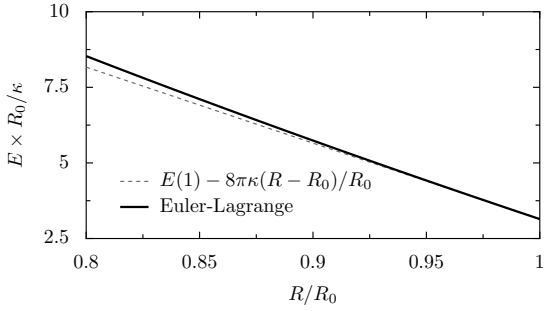

FIG. 7. Bending energy of an incompressible elastic ring of length $2\pi R_0$ (the marginal band) in a sphere of radius $R < R_0$. The solid line represents the numerical solution to the Euler-Lagrange equations (Eq. 28), while the dashed line represents the small deformation approximation, Eq. 38.

$L \to 2\pi R$. Although analytically solving the full shape equation $\mathbf{R}(s)$ is arduous [18] even in this weakly deformed approximation, we can construct a shape equation that satisfies Eq. 30 for small deformation as follows:

$$\mathbf{R} = R \begin{pmatrix} (1-b)\sin t + b\sin 3t \\ (1-b)\cos t - b\sin 3t \\ 2\sqrt{(1-b)b}\cos 2t \end{pmatrix} \tag{31}$$

In which $0 \leq t \leq 2\pi$ is a angle coordinate. For small deformations $b \to 0$, one finds :

$$k_i(s) = 6\sqrt{b}\cos 2s/R + O\left(b^{\frac{3}{2}}\right) \tag{32}$$

$$\ddot{k_i}(s) = \gamma \times 6\sqrt{b}\cos 2s/R + O\left(b^{\frac{3}{2}}\right), \tag{33}$$

with $\gamma = -4$ as expected. From equation 31, we can compute the bending energy of the marginal band :

$$E(R,b) = \int_0^{2\pi} \left(\frac{1}{R^2} + k_i^2\right) \|\partial_t \mathbf{R}\|^2 dt \tag{34}$$

For small deformations $b \to 0$, we have :

$$E(R,b) = \frac{\kappa}{2R}\left(2\pi + 36\pi b + O\left(b^2\right)\right) \tag{35}$$

We can also compute the length of the marginal band, and the energy :

$$L(R,b) = 2\pi R\left(1 + 6b + O\left(b^2\right)\right), \tag{36}$$

$$E(R,L) \to \frac{\kappa}{2R}\left(2\pi + 3\frac{L - 2\pi R}{R}\right) \tag{37}$$

We then find the force exerted by a nearly flat ring on the sphere $L = 2\pi R$:

$$f_B = \lim_{L \to 2\pi R} \partial_R E(R,L) = \frac{8\pi\kappa}{R^2} \tag{38}$$

This result is in agreement with solving the full shape equation (Eq. 28), as illustrated in figure 7. f_b is the force exerted by a nearly flat ring on a sphere ; by construction it is also the critical force at which a ring will buckle. Numerically, we can study ring buckling in two cases : when the ring is undergoing an elastic confinement, and when the ring is confined by a contractile surface.

C. Ring under elastic confinement

Let us consider a ring of length L confined in a a sphere of radius R such that $L = 2\pi(R+\epsilon)$ by an elastic confinement k (see [28] for the implementation of confinement). The confinement force is here $f_c = kn\epsilon$, in which n is the number of points describing the discrete ring. The ring will buckle if $f_c > f_B$; using Eq. 38, we find that the ring will buckle above a critical confinement :

$$k_c = \frac{8\pi\kappa}{n\epsilon R^2}, \tag{39}$$

in which $n = L/ds$, where ds is the segmentation.

D. Ring in a contractile ellipsoid

Using our computed value of f_B, we can compute analytically the critical value of the tension that will buckle a ring in a contractile space, assuming that space to be ellipsoid and near-spherical. For this, we take the very same approach as we did for the bundle in a prolate ellipsoid, although now the ellipsoid is oblate, and the buckling force is that of a ring rather than an open bundle.

$$\sigma^* = \frac{f_B}{\partial_R S(R,R,R_0^3/R^2)} \tag{40}$$

[1] T. Lecuit and P.-F. Lenne, Nature Reviews Molecular Cell Biology **8**, 633 (2007).

[2] L. Goniakowska-Witalinska and W. Witalinski, Journal of cell science **22**, 397 (1976).

[3] K.-G. Lee, T. Miller, I. Anastassov, and W. D. Cohen, Cell biology international **28**, 299 (2004).

[4] S. Patel-Hett, J. L. Richardson, H. Schulze, K. Drabek, N. A. Isaac, K. Hoffmeister, R. A. Shivdasani, J. C. Bulinski, N. Galjart, J. H. Hartwig, *et al.*, Blood **111**, 4605 (2008).

[5] B. Van Deurs and O. Behnke, Zeitschrift für Anatomie und Entwicklungsgeschichte **143**, 43 (1973).

[6] J. G. White, in *Platelets, third edition*, edited by A. D. Michelson (Academic Press, 2013) Chap. 7, pp. 117–144.

[7] J. Joseph-Silverstein and W. D. Cohen, The Journal of cell biology **98**, 2118 (1984).

[8] R. Schroter, R. Z. Filali, A. Brain, P. Jeffrey, and D. Robertshaw, Respiration physiology **81**, 381 (1990).

[9] J. H. Hartwig and M. DeSisto, The Journal of cell biology **112**, 407 (1991).

[10] M. Bathe, C. Heussinger, M. M. Claessens, A. R. Bausch, and E. Frey, Biophysical journal **94**, 2955 (2008).

[11] S. Patel-Hett, H. Wang, A. J. Begonja, J. N. Thon, E. C. Alden, N. J. Wandersee, X. An, N. Mohandas, J. H. Hartwig, and J. E. Italiano, Blood **118**, 1641 (2011).

[12] J. N. Thon, H. Macleod, A. J. Begonja, J. Zhu, K.-C. Lee, A. Mogilner, J. H. Hartwig, and J. E. Italiano Jr, Nature communications **3**, 852 (2012).

[13] W. D. Cohen, D. Bartelt, R. Jaeger, G. Langford, and I. Nemhauser, The Journal of cell biology **93**, 828 (1982).

[14] E. Evans and A. Yeung, Biophysical journal **56**, 151 (1989).

[15] M. P. Stewart, J. Helenius, Y. Toyoda, S. P. Ramanathan, D. J. Muller, and A. A. Hyman, Nature **469**, 226 (2011).

[16] M. Bender, J. N. Thon, A. J. Ehrlicher, S. Wu, L. Mazutis, E. Deschmann, M. Sola-Visner, J. E. Italiano, and J. H. Hartwig, Blood **125**, 860 (2015).

[17] J. G. White and G. Rao, The American journal of pathology **152**, 597 (1998).

[18] K. Ostermeir, K. Alim, and E. Frey, Physical Review E **81**, 061802 (2010).

[19] B. Diagouraga, A. Grichine, A. Fertin, J. Wang, S. Khochbin, and K. Sadoul, The Journal of cell biology **204**, 177 (2014).

[20] M. Kuwahara, M. Sugimoto, S. Tsuji, H. Matsui, T. Mizuno, S. Miyata, and A. Yoshioka, Arteriosclerosis, thrombosis, and vascular biology **22**, 329 (2002).

[21] M. Braun, Z. Lansky, G. Fink, F. Ruhnow, S. Diez, and M. E. Janson, Nature cell biology **13**, 1259 (2011).

[22] F. Gittes, B. Mickey, J. Nettleton, and J. Howard, The Journal of cell biology **120**, 923 (1993).

[23] G. Salbreux, G. Charras, and E. Paluch, Trends in cell biology **22**, 536 (2012).

[24] J.-Y. Tinevez, U. Schulze, G. Salbreux, J. Roensch, J.-F. Joanny, and E. Paluch, Proceedings of the National Academy of Sciences **106**, 18581 (2009).

[25] J.-B. Fournier, D. Lacoste, and E. Raphaël, Physical review letters **92**, 018102 (2004).

[26] H. Turlier, D. Fedosov, B. Audoly, T. Auth, N. Gov, C. Sykes, J.-F. Joanny, G. Gompper, and T. Betz, Nature Physics (2016).

[27] D. M. Kenney and R. Linck, Journal of cell science **78**, 1 (1985).

[28] F. Nedelec and D. Foethke, New Journal of Physics **9**, 427 (2007).

[29] J. H. Hartwig, Platelets **1**, 26 (2002).

[30] W. D. Cohen, Int Rev Cytol **130**, 37 (1991).

[31] J. Guven and P. Vázquez-Montejo, Physical Review E **85**, 026603 (2012).

[32] S. Lux, K. John, and T. E. Ukena, Journal of Clinical Investigation **61**, 815 (1978).

[33] W. D. Cohen, Y. Sorokina, and I. Sanchez, Cell motility and the cytoskeleton **40**, 238 (1998).

[34] J. J. Ward, H. Roque, C. Antony, and F. Nédélec, Elife **3**, e03398 (2014).

[35] J. H. Hartwig, The Journal of Cell Biology **118**, 1421 (1992).

[36] R. C. Carroll and J. M. Gerrard, Blood **59**, 466 (1982).

[37] Z. Li, E. S. Kim, and E. L. Bearer, Blood **99**, 4466 (2002).

[38] N.-K. Lee, A. Johner, and S.-C. Hong, The European Physical Journal E **24**, 229 (2007).

[39] J.-P. Cazenave, P. Ohlmann, D. Cassel, A. Eckly, B. Hechler, and C. Gachet, Platelets and Megakaryocytes: Volume 1: Functional Assays , 13 (2004).

[40] G. Lukinavičius, L. Reymond, E. D'Este, A. Masharina, F. Göttfert, H. Ta, A. Güther, M. Fournier, S. Rizzo, H. Waldmann, *et al.*, Nature methods **11**, 731 (2014).